STRUCTURAL BIOLOGY COMMUNICATIONS

ISSN 2053-230X

Carbonic anhydrase II microcrystals suitable for XFEL studies

Carrie L. Lomelino,[a]‡ Jin Kyun Kim,[b]‡ Cheol Lee,[b] Seon Woo Lim,[b] Jacob T. Andring,[a] Brian P. Mahon,[a]§ Moses Chung,[b] Chae Un Kim[b]* and Robert McKenna[a]*

[a]Department of Biochemistry and Molecular Biology, College of Medicine, University of Florida, Gainesville, FL 32610, USA, and [b]Department of Physics, Ulsan National Institute of Science and Technology, Ulsan 44919, Republic of Korea. *Correspondence e-mail: cukim@unist.ac.kr, rmckenna@ufl.edu

Received 23 February 2018
Accepted 21 April 2018

Edited by P. Dunten, Stanford Synchrotron Radiation Lightsource, USA

‡ These authors should be considered joint first authors.
§ Current address: Laboratory of Chemical Physics, National Institute of Diabetes and Digestive and Kidney Diseases, National Institutes of Health, Bethesda, MD 20892, USA.

Keywords: X-ray free-electron lasers; XFELs; serial femtosecond crystallography; time-resolved crystallography; microcrystals; carbonic anhydrase II.

Recent advances in X-ray free-electron laser (XFEL) sources have permitted the study of protein dynamics. Femtosecond X-ray pulses have allowed the visualization of intermediate states in enzyme catalysis. In this study, the growth of carbonic anhydrase II microcrystals (40–80 µm in length) suitable for the collection of XFEL diffraction data at the Pohang Accelerator Laboratory is demonstrated. The crystals diffracted to 1.7 Å resolution and were indexed in space group $P2_1$, with unit-cell parameters a = 42.2, b = 41.2, c = 72.0 Å, $\beta = 104.2^\circ$. These preliminary results provide the necessary framework for time-resolved experiments to study carbonic anhydrase catalysis at XFEL beamlines.

1. Introduction

Over the last decade, the development of X-ray free-electron lasers (XFELs) has presented new opportunities for experiments in the field of structural biology. With a peak spectral brightness many orders of magnitude higher than a third-generation synchrotron source, and X-ray pulses on the femtosecond timescale, XFEL studies can produce useful diffraction from nanocrystals at room temperature (RT) before the crystal becomes subject to radiation damage (Chapman *et al.*, 2011). As the time resolution of synchrotron sources is limited to ∼100 ps, a femtosecond X-ray pulse provides a means to measure biological reactions that typically occur within picoseconds. Furthermore, the collection of diffraction data at RT is important for the visualization of reaction intermediates, as cryogenic temperatures have been shown to restrict the occupancy of alternate conformational states (Fraser *et al.*, 2009). Thus, serial femtosecond crystallography (SFX) provides the ability to generate 'molecular movies' of enzyme catalytic mechanisms (Spence, 2017).

The emergence of SFX and XFELs in conjunction with photoactivation strategies allows the study of protein dynamics and kinetics in real time, which has been demonstrated in studies of photosystems I and II, myoglobin, photoactive yellow protein (PYP) and bacteriorhodopsin (Nango *et al.*, 2016; Pande *et al.*, 2016; Suga *et al.*, 2017; Kupitz *et al.*, 2014; Levantino *et al.*, 2015). In previous Laue pump–probe time-resolved experiments, large-scale crystals were needed and achieved only 10–12% reaction initiation, whereas ∼40% photoconversion was achieved upon direct exposure of PYP microcrystals to the X-ray beam (Tenboer *et al.*, 2014). The diffraction-before-destruction aspect of SFX and the tendency for low hit rates during data collection therefore demands large volumes of microcrystals for the collection of a complete data set (Chapman *et al.*, 2011). Furthermore, the

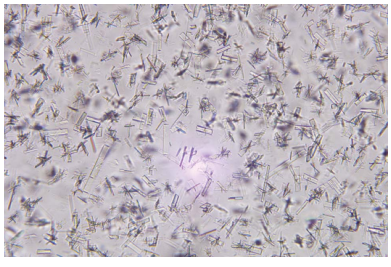

Table 1
Macromolecule-production information.

Source organism	*Homo sapiens*
Expression vector	pET31F1+
Expression host	*E. coli*
Complete amino-acid sequence	MSHHWGYGKHNGPEHWHKDFPIAKGERQSPVDID THTAKYDPSLKPLSVSYDQATSLRILNNGHAF NVEFDDSQDKAVLKGGPLDGTYRLIQFHFHWG SLDGQGSEHTVDKKKYAAELHLVHWNTKYGDF GKAVQQPDGLAVLGIFLKVGSAKPGLQKVVDV LDSIKTKGKSADFTNFDPRGLLPESLDYWTYP GSLTTPPLLECVTWIVLKEPISVSSEQVLKFR KLNFNGEGEPEELMVDNWRPAQPLKNRQIKAS FK

microcrystals must be homogenous in size not only to aid delivery but also to ensure uniform photoactivation.

Carbonic anhydrase II (CA II), a zinc metalloenzyme that catalyzes the reversible hydration of CO_2, is one of the fastest known enzymes, with a k_{cat} of 10^6 s^{-1} (Steiner *et al.*, 1975). This reaction follows a classic two-step ping-pong enzymatic mechanism. In the hydration direction, a zinc-bound hydroxide performs a nucleophilic attack on CO_2, resulting in a zinc-bound HCO_3^- product that is subsequently displaced by a water molecule. The zinc-bound solvent is regenerated through a proton-transfer mechanism facilitated by a histidine residue at the entrance to the active site (Boone *et al.*, 2014).

Although this reaction has been extensively studied and X-ray crystal structures of CA II in complex with substrate and product have been elucidated, there is still little structural information regarding the dynamics of the catalytic mechanism (Domsic *et al.*, 2008; Domsic & McKenna, 2010; Kim *et al.*, 2016, 2018; Fierke *et al.*, 1991). Hence, the use of pump–probe, time-resolved SFX (TR-SFX) would be the preferred methodology to visualize the pathways of substrate/product entry/exit from the active site. This can be achieved using photoactivatable compounds such as 3-nitrophenylacetic acid (3NPAA), which releases CO_2 upon photolysis (λ = 350 nm; Figs. 1*a* and 1*b*). Therefore, CA II is an excellent candidate for the use of SFX–XFEL studies.

Here, we demonstrate the production of CA II microcrystals suitable for the collection of XFEL diffraction data and present preliminary XFEL data and processing results.

2. Materials and methods

2.1. Macromolecule production

The expression and purification of CA II were performed as described previously (Tanhauser *et al.*, 1992; Pinard *et al.*, 2013). In brief, CA II was expressed in *Escherichia coli* BL21 (DE3) competent cells *via* IPTG induction (Table 1). The protein was then purified using affinity chromatography with *p*-(aminomethyl)-benzenesulfonamide resin. The purity was verified by SDS–PAGE and the concentration was determined *via* UV–Vis spectroscopy.

2.2. Crystallization

Crystals of CA II were grown at 298 K using the hanging-drop vapor-diffusion method with a precipitant solution consisting of 1.6 *M* sodium citrate, 50 m*M* Tris pH 7.8. Upon visual inspection, a single high-quality crystal (~200 × 50 × 50 µm) was transferred from the crystal drop into a new 10 µl drop of precipitant solution and crushed using a needle. The needle was then immersed into a secondary 10 µl droplet of precipitant solution to dilute the crystals and create a CA II seed stock.

CA II microcrystals were grown at 298 K utilizing a combination of seeding and batch crystallization methods by adding CA II seed stock and purified protein directly to the

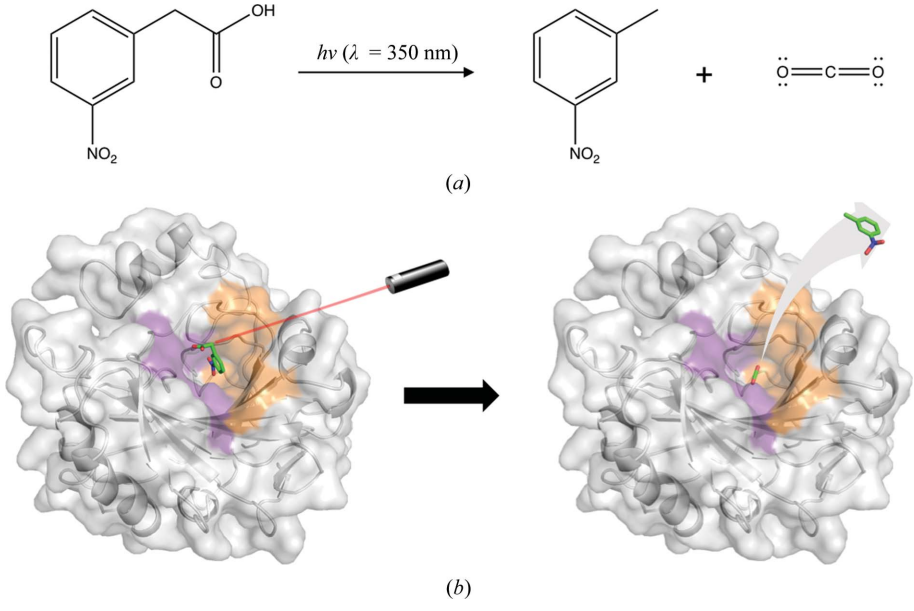

Figure 1
(*a*) Scheme for CO_2 generation *via* photolysis of 3NPAA. (*b*) Surface representation of CA II in complex with 3NPAA (unpublished data) which can be activated with a 350 nm laser pulse to free CO_2.

precipitant solution. In a 24-well culture plate, 5 µl seed stock, 300 µl CA II (30 mg ml^{-1}) and 1200 µl precipitant solution were added to each well as described previously (Mahon *et al.*, 2016). Microcrystal growth was observed after 12 h. The microcrystal suspension was diluted in precipitant solution (1:4 ratio) and syringe-filtered through a metal filter, removing crystals of greater than 100 µm in length. After five successive filtrations, the microcrystal suspension was concentrated by centrifugation at ∼840*g* for 5 min. The microcrystals were then mixed with monoolein (100%, Hampton Research) in a 1:1 ratio in gas-tight syringes and transferred into a lipid cubic phase (LCP) injector (Weierstall *et al.*, 2014) for data collection.

2.3. Data collection and processing

Diffraction data were collected at the Coherent X-ray Imaging (CXI) station at Pohang Accelerator Laboratory XFEL (PAL-XFEL; Kang *et al.*, 2017). The CXI station at PAL-XFEL is specifically designed for SFX and time-resolved SFX experiments, with Kirkpatrick–Baez (KB) mirrors for ∼2 µm microfocusing, an LCP injector system for microcrystal delivery, an optical (pump) femtosecond laser and capabilities to collect data at a 60 Hz repetition rate. For our data collection, we utilized single-shot X-ray pulses at 10 Hz and a microfocus of 5 µm diameter. The X-ray pulse widths were 20 fs at 1.2 × 10^{11} photons per pulse (photon energy = 9.715 keV). The subsequent X-ray diffraction data were collected on a Rayonix detector with a readout rate of 10 Hz. The microcrystal suspension in monoolein allowed sample injection using an isocratic flow mode at a flow rate of 150 nl min^{-1}. The injector diameter was 100 µm and the sample-to-detector distance was 130 mm.

Three methods of data pre-processing were tested with *NanoPeakCell*: methods A, B and C using images containing more than ten detector pixels with $I > 10\,000$, $I > 5000$ and $I > 1000$, respectively (Coquelle *et al.*, 2015). *CrystFEL* was utilized for data indexing using the *peakfinder*8 and *MOSFLM* functions (White *et al.*, 2012).

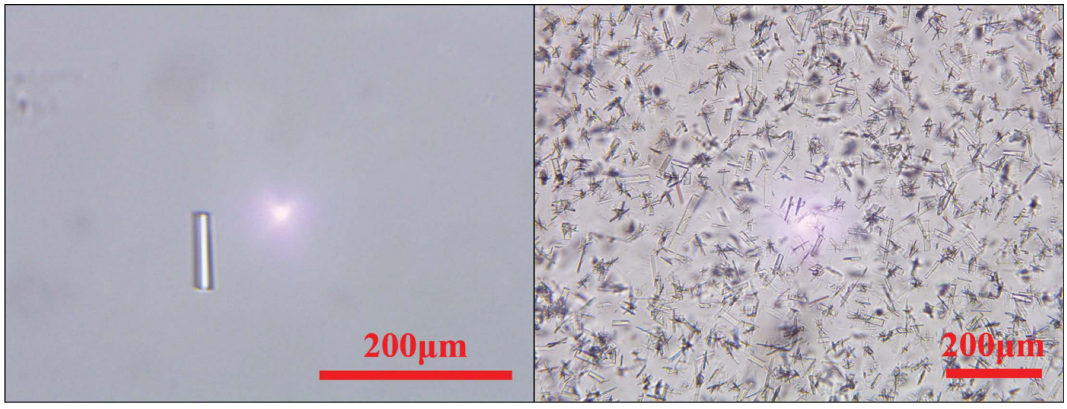

(*a*) (*b*)

Figure 2
(*a*) CA II crystals grown *via* batch crystallization. (*b*) CA II microcrystals grown by combining seeding and batch crystallization techniques.

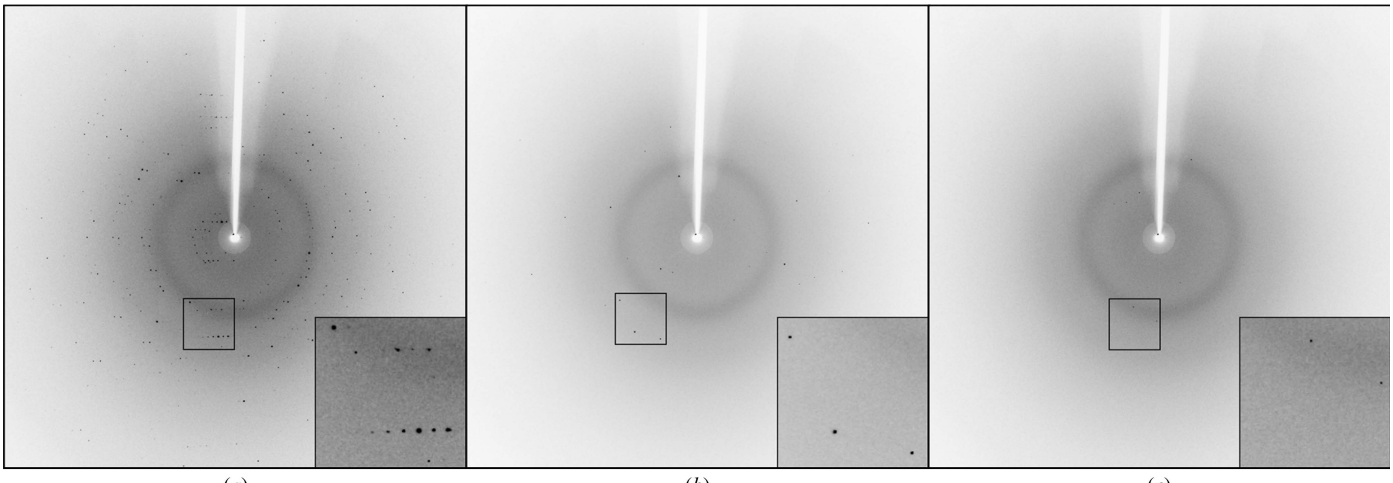

(*a*) (*b*) (*c*)

Figure 3
XFEL diffraction of CA II microcrystals. Representative images of the data used for methods A, B and C with more than ten detector pixels with $I > 10\,000$, $I > 5000$ and $I > 1000$, respectively.

Table 2
XFEL diffraction data statistics.

Values in parentheses are for the outer shell.

Method	A	B	C
Wavelength (keV)	9.715		
X-ray focus (μm)	5 × 5		
Pulse energy/fluence at sample (photons per pulse)	1.2×10^{11}		
Space group	Monoclinic, $P2_1$		
Unit-cell parameters (Å, °)	a = 42.2, b = 41.2, c = 72.0, β = 104.2		
Total No. of images	380 000		
No. of sorted images	199	812	15996
No. of indexed images	190	782	9629
No. of unique reflections	5856	19024	24451
Resolution limits (Å)	69.8–1.7 (1.74–1.70)		
Completeness (%)	23.0 (6.9)	74.6 (35.0)	99.8 (98.3)
$\langle I/\sigma(I)\rangle$	5.2 (5.0)	4.5 (2.1)	2.4 (1.1)
$R_{\rm split}$†	0.965	0.830	0.366
Wilson B factor (Å^2)	18.2	23.5	29.3
R.m.s.d., bonds (Å)	0.011	0.011	0.013
R.m.s.d., angles (°)	1.58	1.58	1.74

† $R_{\rm split} = 2^{-1/2}(\sum |I_{\rm even} - I_{\rm odd}|)/[1/2 \sum (I_{\rm even} - I_{\rm odd})]$ (White *et al.*, 2012).

3. Results and discussion

The batch crystallization method, in which purified CA II was directly mixed with precipitant solution, resulted in only a few CA II crystals (Fig. 2*a*). Hence, this method alone was inadequate for producing the large volumes of crystals necessary for XFEL experiments and delivery *via* an LCP injector. Therefore, microcrystals were grown *via* seeding in conjunction with batch crystallization, promoting multiple crystal nucleation points (Fig. 2*b*). As this method resulted in a mixture of crystal sizes, syringe-driven filtration was used to exclude larger crystals, resulting in crystals ranging between 40 and 80 μm in size. The microcrystal suspension was combined with monoolein as a homogenous mixture that was effectively injected *via* an LCP injector without clogging.

The CA II microcrystals were shown to diffract to a maximal resolution of 1.7 Å and belonged to space group $P2_1$, with unit-cell parameters a = 42.2, b = 41.2, c = 72.0 Å, β = 104.2° (Fig. 3). A total of 380 000 images were collected in 4 h, of which 199, 812 and 15 996 images were selected during pre-processing using methods A, B and C, respectively. This resulted in hit rates of 0.05, 0.21 and 4.21%, respectively (Table 2).

Overall, these experiments demonstrate the successful growth of CA II microcrystals suitable for XFEL data collection. Furthermore, our diffraction data confirm the feasibility of pump–probe TR-SFX experiments to study the catalytic mechanism of CA II in conjunction with photoactivatable compounds.

Acknowledgements

The experiment was performed on the NCI beamline of PAL-XFEL. The authors would like to acknowledge the expertise and guidance provided by the PAL-XFEL experimental staff.

Funding information

Funding for this research was provided by: National Research Foundation of Korea (award No. 2014R1A2A1A11051254; award No. 2016R1A5A1013277).

References

Boone, C. D., Pinard, M., McKenna, R. & Silverman, D. (2014). *Carbonic Anhydrase: Mechanism, Regulation, Links to Disease, and Industrial Applications*, edited by S. C. Frost & R. McKenna, pp. 31–52. Dordrecht: Springer.
Chapman, H. N. *et al.* (2011). *Nature (London)*, **470**, 73–77.
Coquelle, N., Brewster, A. S., Kapp, U., Shilova, A., Weinhausen, B., Burghammer, M. & Colletier, J.-P. (2015). *Acta Cryst.* D**71**, 1184–1196.
Domsic, J. F., Avvaru, B. S., Kim, C. U., Gruner, S. M., Agbandje-McKenna, M., Silverman, D. N. & McKenna, R. (2008). *J. Biol. Chem.* **283**, 30766–30771.
Domsic, J. F. & McKenna, R. (2010). *Biochim. Biophys. Acta*, **1804**, 326–331.
Fierke, C. A., Calderone, T. L. & Krebs, J. F. (1991). *Biochemistry*, **30**, 11054–11063.
Fraser, J. S., Clarkson, M. W., Degnan, S. C., Erion, R., Kern, D. & Alber, T. (2009). *Nature (London)*, **462**, 669–673.
Kang, H.-S. *et al.* (2017). *Nat. Photon.* **11**, 708–713.
Kim, C. U., Song, H., Avvaru, B. S., Gruner, S. M., Park, S. & McKenna, R. (2016). *Proc. Natl Acad. Sci. USA*, **113**, 5257–5262.
Kim, J. K., Lomelino, C. L., Avvaru, B. S., Mahon, B. P., McKenna, R., Park, S. & Kim, C. U. (2018). *IUCrJ*, **5**, 93–102.
Kupitz, C. *et al.* (2014). *Nature (London)*, **513**, 261–265.
Levantino, M., Schirò, G., Lemke, H. T., Cottone, G., Glownia, J. M., Zhu, D., Chollet, M., Ihee, H., Cupane, A. & Cammarata, M. (2015). *Nature Commun.* **6**, 6772.
Mahon, B. P., Kurian, J. J., Lomelino, C. L., Smith, I. R., Socorro, L., Bennett, A., Hendon, A. M., Chipman, P., Savin, D. A., Agbandje-McKenna, M. & McKenna, R. (2016). *Cryst. Growth Des.* **16**, 6214–6221.
Nango, E. *et al.* (2016). *Science*, **354**, 1552–1557.
Pande, K. *et al.* (2016). *Science*, **352**, 725–729.
Pinard, M. A., Boone, C. D., Rife, B. D., Supuran, C. T. & McKenna, R. (2013). *Bioorg. Med. Chem.* **21**, 7210–7215.
Spence, J. C. H. (2017). *IUCrJ*, **4**, 322–339.
Steiner, H., Jonsson, B. H. & Lindskog, S. (1975). *Eur. J. Biochem.* **59**, 253–259.
Suga, M. *et al.* (2017). *Nature (London)*, **543**, 131–135.
Tanhauser, S. M., Jewell, D. A., Tu, C. K., Silverman, D. N. & Laipis, P. J. (1992). *Gene*, **117**, 113–117.
Tenboer, J. *et al.* (2014). *Science*, **346**, 1242–1246.
Weierstall, U. *et al.* (2014). *Nature Commun.* **5**, 3309.
White, T. A., Kirian, R. A., Martin, A. V., Aquila, A., Nass, K., Barty, A. & Chapman, H. N. (2012). *J. Appl. Cryst.* **45**, 335–341.